# $K$-Mesonic X Rays and $K^-$ Absorption in Liquid Helium*†

DANIEL N. MICHAEL‡
*Argonne National Laboratory, Argonne, Illinois*
*and*
*The University of Chicago, Chicago, Illinois*
(Received 20 February 1967)

An experiment is described in which $K$-mesonic x rays were observed in $He^4$. The experiment was performed in an unseparated beam by selecting $K^-$ stopping in a liquid-helium target with a system of fast counters, and observing the x rays in a gas proportional counter gated by the stopping signal. An x-ray line was observed at $6.5\pm0.4$ keV and was identified to be the $L_\alpha$ transition of kaonic helium. There was also some evidence for a second line in the spectrum at $35.4\pm0.9$ keV, assumed to be the $K_\alpha$, with an intensity of $(49\pm22)\%$ relative to the $L_\alpha$. The absolute yield of the $L_\alpha$ transition was determined to be $(85\pm25)\%$. This directly establishes that most $K^-$ are absorbed from low-lying states in helium. A simple model was constructed for the de-excitation of kaonic helium and was used to calculate the atomic cascade. With reasonable assumptions about the initial population of states, this calculation gave values for both the $L_\alpha$ yield and the cascade time consistent with the experimental values, and was used to predict a nuclear-capture schedule for $K^-$ in helium. From the line assumed to be the $K_\alpha$, it was possible to deduce an upper limit for the complex-energy shift to the $1S$ level from the $\bar{K}$-$\alpha$ interaction, and a value for the absorption rate from the $2P$ level.

## I. INTRODUCTION

RECENTLY $K$-mesonic x rays have been observed[1] in an experiment in which $K^-$ were brought to rest in a large liquid-helium target. In this experiment, the existence of one x-ray line in the observed spectrum was firmly established, and its measured energy corresponded to that of the $L_\alpha$ transition of kaonic helium. There was also evidence for the presence of a second x-ray line, believed to be the $K_\alpha$ transition. The absolute yields of these transitions have been given in a preliminary report.[2] In the present paper, we describe the experiment and its results more in detail, and explore what can be learned from these results about the nuclear absorption process of $K^-$ in liquid helium.

The problem of negative-meson absorption in helium has been discussed in the literature for several years.[3–5] The only experimental work to shed light on the problem has been the measurements of absorption times made in liquid-helium bubble chambers. Measurements have been reported both for $\pi^-$,[3,4] and for $K^-$[4], and the absorption times were found to be much longer than the corresponding times for $\pi^-$ [6] and $K^-$ [7] in liquid hydrogen, or for $\pi^-$ in liquid deuterium.[8] A qualitative difference was expected, but important features of the absorption process cannot be obtained from the absorption times alone. It was well known that in hydrogen, Stark mixing within the principal levels leads to a large amount of $S$-state capture while the mesons are still at high atomic levels.[9–11] In helium, one expected much less Stark mixing, since the $K\alpha^+$ ion cannot approach the nuclei of other atoms as closely as the neutral $Kp$ atom; however, the question of the precise capture schedule had not yet been settled.[5] The absolute yield of the $L_\alpha$ transition seen in the present experiment directly establishes that the amount of capture from the higher levels is small. Using this as a guide, we have investigated the atomic cascade and have calculated a capture schedule for $K^-$ in helium.

The remaining sections have been set up according to the following plan: in Sec. II, the experimental apparatus is described in detail and the observed x-ray spectrum is discussed; Sec. III describes how the absolute yield of the x rays was determined; in Sec. IV, the atomic cascade is investigated and a capture schedule is calculated; and in Sec. V, the results of the experiment are summarized and the main conclusions which can be drawn from them are given.

* Work performed under the auspices of the U. S. Atomic Energy Commission.
† A thesis submitted in partial fulfillment of the requirements for the Ph.D. degree in the Department of Physics, The University of Chicago.
‡ Present address: Brookhaven National Laboratory, Upton, Long Island, New York.
[1] G. R. Burleson, D. Cohen, R. C. Lamb, D. N. Michael, R. A. Schluter, and T. O. White, Jr., Phys. Rev. Letters **15**, 70 (1965).
[2] D. N. Michael, Bull. Am. Phys. Soc. **10**, 1123 (1965).
[3] M. M. Block, T. Kikuchi, D. Koetke, J. Kopelman, C. R. Sun, R. Walker, G. Culligan, V. L. Telegdi, and R. Winston, Phys. Rev. Letters **11**, 301 (1963); J. G. Fetkovich and E. G. Pewitt, *ibid.* **11**, 290 (1963).
[4] M. M. Block, J. B. Kopelman, and C. R. Sun, Phys. Rev. **140**, B143 (1965).
[5] J. E. Russell, Proc. Phys. Soc. (London) **85**, 245 (1965).
[6] J. H. Doede, R. H. Hildebrand, M. H. Israel, and M. R. Pyka, Phys. Rev. **129**, 2808 (1963); E. Bierman, S. Taylor, E. L. Koller, P. Stamer, and T. Huetter, Phys. Letters **4**, 351 (1963).
[7] R. Knop, R. A. Burnstein, and G. A. Snow, Phys. Rev. Letters **14**, 767 (1965); M. Cresti, S. Limentani, A. Loria, L. Peruzzo, and R. Santangelo, *ibid.* **14**, 847 (1965).
[8] J. H. Doede, R. H. Hildebrand, and M. H. Israel, Phys. Rev. **136**, B1609 (1964).
[9] T. B. Day, G. A. Snow, and J. Sucher, Phys. Rev. Letters **3**, 61 (1959); Phys. Rev. **118**, 864 (1960).
[10] J. E. Russell and G. L. Shaw, Phys. Rev. Letters **4**, 369 (1960).
[11] M. Leon and H. A. Bethe, Phys. Rev. **127**, 636 (1962).

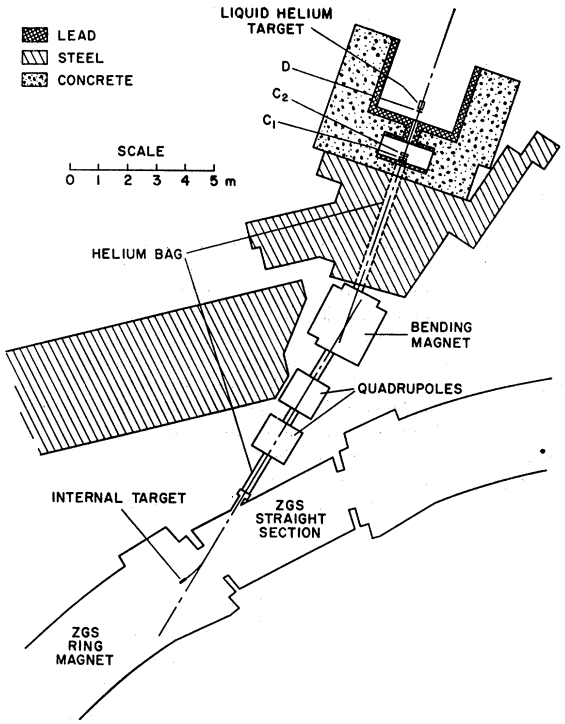


FIG. 1. Beam layout for the experiment. Kaons were transported for 18.0 m at 840 MeV/$c$, selected electronically, and brought to rest in a liquid-helium target. The beam was not separated.

## II. EXPERIMENT

The mesonic x rays were observed in an experiment performed in a low-momentum, unseparated $K^-$ beam at the Argonne Zero Gradient Synchrotron (ZGS). The experiment has been briefly described in Ref. 1. A scale drawing of the low-momentum beam is shown in Fig. 1. Negative particles were selected near 0° from an internal target of the ZGS and transported for 18.0 m at 840 MeV/$c$ in a helium atmosphere. The $K^-$ in the beam were selected with counters, slowed by a copper degrader, and brought to rest in a liquid-helium target. The x rays were observed in a gas proportional counter which was gated on the stopping $K^-$ signal. A summary of the characteristics of this beam and some typical rates are given in Table I.

A drawing of the helium target and counter geometry is shown in Fig. 2. Two inverse-threshold Čerenkov counters,[12] $C_1$ and $C_2$, were used to select kaons ($\beta=0.863$ for 840 MeV/$c$) in the incident beam. These two counters were identical; each consisted of a 7.6-cm thick Lucite radiator with four 56AVP photomultipliers masked to accept Čerenkov light in the Lucite at an angle of 38.9° from the beam axis, corresponding to $\beta=0.863$. Pion light (47.9°, $\beta=0.987$) was rejected by total internal reflection in the lucite. Pion contamination of this signal was caused by nuclear interactions and delta rays in the Lucite: about one pion in $10^4$ was found to register in the two counters in coincidence, giving a kaon to pion ratio of about 6/1 in this signal.

After the Čerenkov counters, the beam was slowed by a copper degrader of mean thickness of 188 g/cm$^2$. The degrader was designed with a 15.2° wedge to correct for the lateral dispersion of the beam (1.06 MeV/$c$ cm at the degrader). Since a large portion of the kaons were lost by nuclear interactions in the degrader (see Table I), it was necessary to provide a subsequent means of selection. The surviving kaons were about four times minimum ionization, while the surviving pions had a

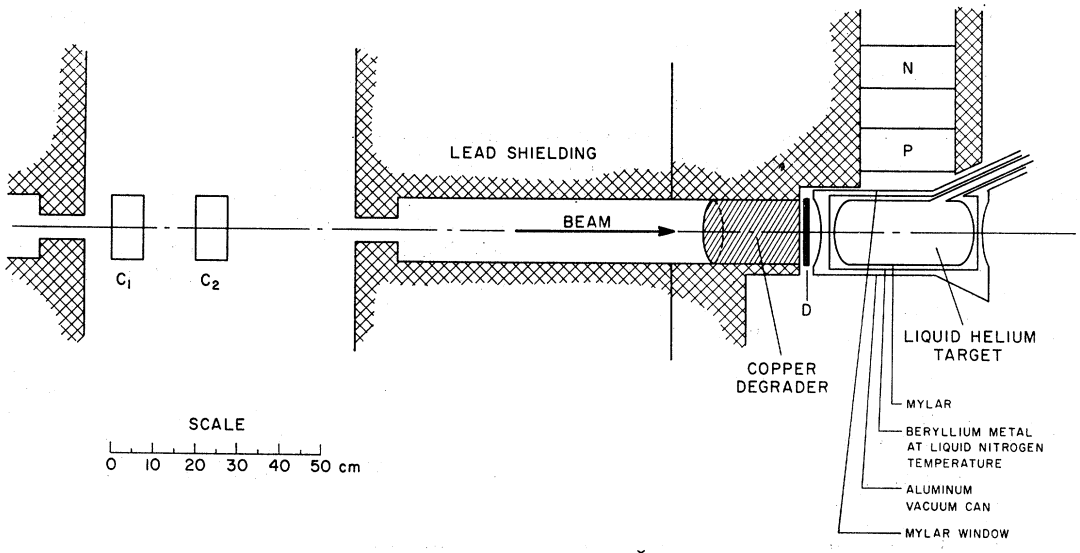


FIG. 2. Target and detector positions in the experiment. $C_1$ and $C_2$ were Čerenkov counters selecting incident kaons, and $D$ was a scintillator with a high-amplitude threshold selecting kaons out of the degrader. The x rays were detected in P, a gas proportional counter, gated on $C_1C_2D$.

[12] J. Farr, Argonne National Laboratory, ANL-HEP Report, 1964 (unpublished).

residual momentum of about 500 MeV/$c$, high enough still to be near minimum ionization. A 1.27-cm thick plastic scintillator $D$, with an amplitude threshold set to be just below four times minimum ionization, was used to select kaons emerging from the degrader. The complete gate signal used for the observation of the x rays was the coincidence $C_1C_2D$. The kaon-to-pion ratio of this signal was about $\frac{1}{4}$.

The target[13] held 6 liters of liquid helium, with a thickness along the beam of 4.0 g/cm$^2$. The cryostat was designed with especially thin windows between the helium and the x-ray detector so that the x-ray absorption would be as small as possible. The total thickness of material between the liquid helium and the gas of the proportional counter consisted of: 0.14 mm of Mylar, and 0.10 mm of beryllium metal (heat shield).

The proportional counter used to detect the x rays is shown as $P$ in Fig. 2. A proportional counter was used several years ago by West and Bradley[14] to observe $\pi$-mesonic x rays. The counter used in the present experiment followed many similar design features; however, it was designed for a somewhat lower energy range, ~5 keV to 40 to include the $K$ and $L$ transitions of kaonic helium. A drawing of the counter is given in Fig. 3(a). It was filled with argon "counting gas" (10% methane, controlled concentration) at 1 atm. Fresh gas was continually circulated through the counter at a slight overpressure to eliminate contamination. The center wires were 0.152 mm (0.006 in.) diameter spring steel music wire; deviations in the uniformity of the diameter of this wire were measured to be no greater than ±1%. There were two wires in the counter, as shown in Fig. 3(a), and a ground plane was placed midway between them. Field tubes 1.9 cm (0.75 in.) in diameter were situated at each end of the wires, and the voltages of these were adjusted separately to give a uniform gain throughout the active volume of the chamber. The gain throughout the active volume was measured using a collimated x-ray source and was found to be constant to within ±1.5% when the field-tube voltages were adjusted properly. The active volume [shown in Fig. 3(a)] was sharply defined by the

TABLE I. Some characteristics of the low-momentum, unseparated $K^-$ beam.

| | |
|---|---|
| Internal target | 0.32×0.32×9.78 cm, copper |
| Solid angle acceptance | $8\times10^{-4}$ sr |
| Central momentum | 840 MeV/$c$ |
| Momentum acceptance | ±1.0% |
| Beam length, to degrader | 18.0 m |
| Survival of $K^-$ from decay | 0.060 |
| Degrader | 188 g/cm$^2$, copper |
| Survival of $K^-$ from losses in degrader | 0.12 |
| Liquid-helium target | 4.0 g/cm$^2$ |
| Typical rates[a]: | |
| Internal proton beam | $3.5\times10^{11}$ |
| Negatives into degrader | $8\times10^6$ |
| $K^-$ into degrader | $2.8\times10^3$ |
| $K^-$ stopped in target | 15 |
| Typical spill time | 0.10 sec |

[a] Rates given are per ZGS pulse. The repetition cycle was 4.0 sec.

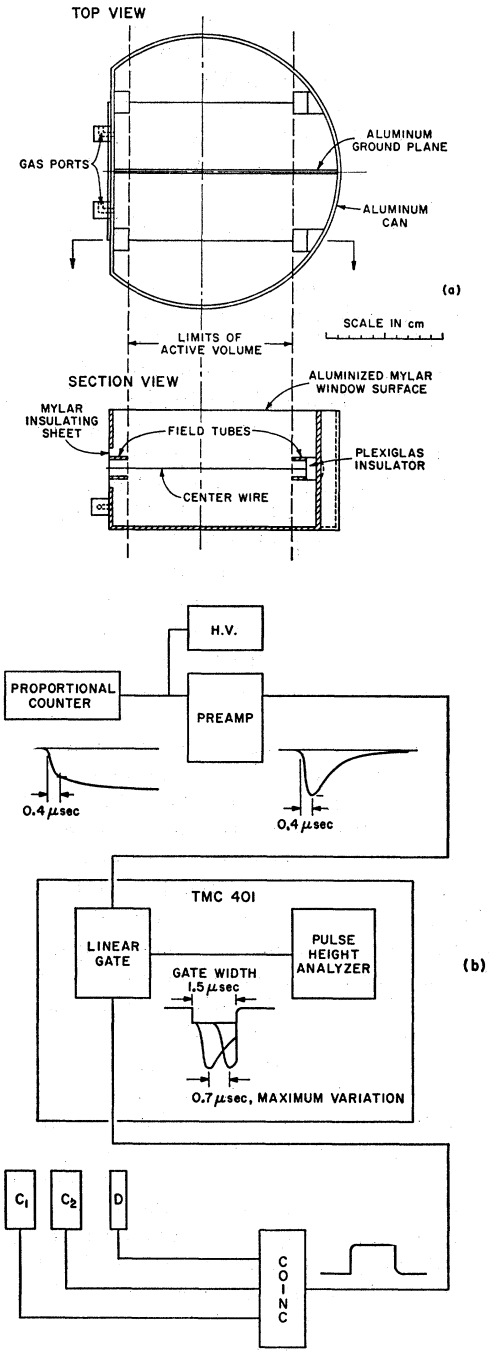


FIG. 3. (a) Diagram of the proportional counter. (b) Block diagram of the electronics.

[13] R. C. Lamb, H. F. Ludwig, C. J. Crookes, W. A. Siembieda, A. Tamosaitis, R. A. Schulter, and J. Farr, Bull. Am. Phys. Soc. 9, 640 (1964); also H. F. Ludwig and A. Tamosaitis, Argonne National Laboratory, ANL-HEP Report No. HL/AT-1, 1964 (unpublished).

[14] D. West and E. Bradley, Phil. Mag. (Ser. 8) 2, 957 (1957).

field tubes and had an area of 300 $cm^2$ at the window surface of the counter. The window surface was of 0.05 mm (0.002 in.) aluminized Mylar, which gave greater than 80% transmission for x rays $\gtrsim 5$ keV. The counter was 10.2 cm (0.16 $g/cm^2$) thick, which gave nearly 100% absorption for x rays $\lesssim 15$ keV, and 24% absorption for 35 keV.

The center wires were at a positive potential of 3000 V, the field tubes were at about 1200 V, and the outer conducting can and window surface were grounded. A block diagram of the electronics system is given in Fig. 3(b). The charge pulses from the center wires were collected onto a capacitance of about 25 pF (76 cm of RG-114 cable plus $\sim 10$ pF stray input circuit capacitance). The resulting voltage pulse was shaped and amplified in a low-noise preamp system (ANL Electronics Division, A-168) and stored in a 200-channel pulse-height analyzer (TMC 401). The preamp gave a pulse which rose to a peak value in 0.4 $\mu$sec and had an exponential trailing edge with a 0.6 $\mu$sec time constant. The gain of the preamp was about 80, its noise level was below 0.05 mV, and the output pulse height was about 3.5 mV/keV. The energy resolution of this system was measured to be 11.2% (full width at half maximum) for 22.2 keV and was inversely proportional to the square root of the energy over the designed energy range. The linearity of the system, as determined by three different x-ray sources ($Fe^{55}$, $Cd^{109}$, $Cs^{137}$), was better than $\pm 0.3\%$ over the designed energy range. Gain variations seen when a source was moved throughout the region of space corresponding to the position of the liquid-helium target were less than 0.5%.

For the observation of the kaonic x rays, the pulse-height analyzer was gated by the stopping $K^-$ signal, $C_1C_2D$, as shown in Fig. 3(b). During the run, the timing of the gate signal relative to the proportional counter pulse was adjusted by observing on an oscilloscope the timing between the two simultaneous $\gamma$ rays from $Co^{60}$: one which was detected in the scintillator $D$, and the other which was detected in the proportional counter. The timing adjusted in this manner did not affect the gain or resolution of the system when the spectrum from an x-ray source was recorded with self-gating of the pulses from the proportional counter. Although no direct observation was made of the resolution with external gating, the resolution was not expected to be affected by the gating because the sensitive time of the pulse-height analyzer was adjusted to be long enough to accept the maximum variations in the time of arrival of the proportional-counter pulses. These variations (caused by electron collection time variations over the sensitive volume of the counter) were observed with $Co^{60}$ to be a maximum of 0.7 $\mu$sec. As shown in Fig. 3(b), the sensitive time of the gated pulse-height analyzer was long enough to include this time variation: the pulses rose to full amplitude in 0.4 $\mu$sec, and the sensitive time was 1.5 $\mu$sec. Since the proportional counter was exposed to a flux of charged particles from the degrader and the target (see Fig. 2), the pulse rate of the counter was monitored during the run to verify that gain variations from pulse pile-up remained negligible. The maximum rate seen during the run was $3.4\times 10^4$ $sec^{-1}$; thus, the probability for pile-up in the sensitive time of the gate pulse-height analyzer was less than 5%. Energy calibrations with an x-ray source taken during the beam spill showed no change in gain at these rates.

The x-ray lines from kaonic helium were found by taking the difference between the spectrum recorded with the target full of helium and the spectrum recorded with the target vessel in place, but empty. The target-full data were taken in six individual runs over a period of about eight hours, and the target-empty data were taken in one run lasting about 90 min. The energy calibration was periodically established with the lines from two x-ray sources: the 5.9-keV line of $Fe^{55}$, and the 22.2-keV line of $Cd^{109}$. The energy calibration of each individual run, including the effect of gain drift, was established to an accuracy of about $\pm 2\%$, and this number was taken to be an estimate of the over-all uncertainty in gain. Because of long-term gain drifts, the energy gains of the six individual target-full spectra differed by as much as 10%; therefore, before these spectra were summed, each was corrected to have the same gain as for the target-empty run. These drifts in gain were caused by changes in the gas density in the proportional counter over long periods of time from temperature and barometric-pressure variations. The base line (channel for zero energy) was established by the two sources to an accuracy of $\pm 1.5$ channel; it remained stable throughout the runs.

The spectrum which is the sum of the six gain-corrected, target-full runs and the spectrum from the target-empty run are both shown in Fig. 4(a). In obtaining the difference between these two spectra, the target-empty spectrum was scaled to give the same total number of counts as the target-full spectrum in the interval from channel 40 to 188. The difference spectrum is shown in Fig. 4(b). In this spectrum, three adjacent channels have been combined in order to make the peaks more apparent to the eye, and the amount of statistical uncertainty in the difference is indicated by the brackets at several representative points. In Fig. 4(c), lines are shown from the two calibration sources taken during the run, and from a third source, $Cs^{137}$ at 32.2 keV, which was used to check the linearity of the system. The energy scale deduced from these sources is shown beneath the figures.

The difference spectrum, Fig. 4(b), has a pronounced peak centered near channel 20. The total number of counts in this peak, summed from channel 9 to 30, is $1975\pm 465$. The center of the peak was determined by locating the channel position which gave the number of counts to the left of it (to channel 9) equal to the

number to the right of it (to channel 30). For this peak, the center was located at channel (18.8±1.4); the uncertainty is statistical. From the energy calibrations, the gain was established to be 0.208±0.004 keV/channel, and the base line was located at channel (−12.3±1.5). The energy of this line, therefore, was 6.5±0.4 keV. The expected energy of the $L_\alpha$ transition in kaonic helium is 6.5 keV. The various contributions to the quoted error were the following: 0.29-keV statistical uncertainty, 0.13-keV uncertainty in gain, 0.31-keV uncertainty in base line, and 0.02-keV uncertainty in linearity. These uncertainties have been combined in quadrature. In order to determine the width of this line, a normal curve was fitted to the peak by the method of least squares.[15] This gave a full width at half maximum of $10.4_{-3.5}^{+5.2}$ channels, compared with an expected width of 7.4 channels. This method, of course, gave results for the center position of the peak and the area under the peak which were consistent with those values quoted above.

In the region around channel 155, there is possibly an indication of a second peak in the spectrum. In order to investigate this more quantitatively, a straight line was fit to the spectrum, by the method of least squares,[15] in two different intervals: first from channel 52 to 120, where no peak is apparent; and then from channel 120 to 188, in the region of the suspected peak. The results of these fits, shown in the first two rows of Table II, give values of $\chi^2$ corresponding to a confidence level of 0.56 in the lower interval, and 0.16 in the upper interval, indicating a fairly low probability that the peak around channel 155 is a statistical fluctuation from a straight line. On the other hand, the best normal-curve fit to the spectrum in this upper interval gives a $\chi^2$ corresponding to a confidence level of 0.60 (third row of Table II); moreover, this fit gave a value for the width which was consistent with the expected instrumental resolution for a line in this region. If the zero level of the difference spectrum is taken to be fixed by the subtraction procedure, the probability for a statistical fluctuation is lower, as shown in the last four rows of Table II. In the 30 channels centered around the suspected peak, the line constrained to the zero level gives a $\chi^2$ corresponding to a confidence level of 0.05, whereas the best-fit normal

TABLE II. Results of various least-squares fits to the difference spectrum, Fig. 4(b), in the region of the suspected $K_\alpha$ peak.

| Range of fit (channel numbers) | Hypothesis | Number of degrees of freedom | $\chi^2$ | $\chi^2$ confidence level |
|---|---|---|---|---|
| 52–120 | Straight line (best fit) | 67 | 64.73 | 0.56 |
| 120–188 | Straight line (best fit) | 67 | 74.25 | 0.16 |
| 120–188 | Normal curve (best fit) | 66 | 62.62 | 0.60 |
| 120–149 | Zero line | 30 | 25.78 | 0.69 |
| 143–174 | Zero line | 30 | 43.92 | 0.05 |
| 169–188 | Zero line | 30 | 32.17 | 0.37 |
| 143–174 | Normal curve (best fit) | 27 | 24.31 | 0.66 |

[15] We note that the difference spectrum given in Fig. 4(b) has three adjacent channels combined so that the peaks show more clearly. The maximum amount of information on the shape of the line is contained in the channel-by-channel difference spectrum, and it was this spectrum which has been used in all least-squares fitting.

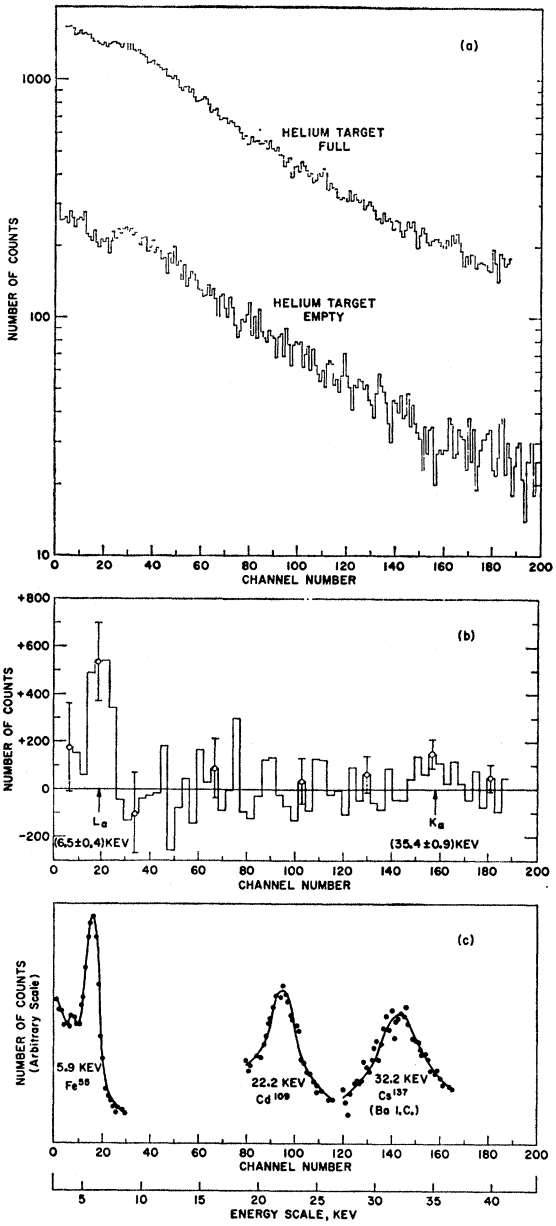


FIG. 4. (a) The pulse-height spectra from the gated proportional counter taken with the target full of helium and with the target vessel in place, but empty. (b) The target-full spectrum with the target-empty spectrum scaled (see text), and subtracted as background. The combined counts in three adjacent channels have been plotted. The brackets indicate the amount of statistical uncertainty. The arrows mark the centers of the peaks assumed to be the $L_\alpha$ and $K_\alpha$ transitions of kaonic helium. (c) The spectra from three x-ray sources used for calibration.

curve gives 0.66. In all other 30-channel intervals of the spectrum above channel 40, the zero line gives $\chi^2$ sums corresponding to confidence levels ranging from 0.3 to 0.7.

The assumption of fixing the zero line in these tests, of course, depends upon how well the background subtraction is known. If we accept the target-empty spectrum as the appropriate background, then the statistical uncertainty in the zero line is determined by the uncertainty in the scale factor multiplying the target-empty spectrum. This scale factor, it will be recalled, is the ratio of the total number of counts in the interval from channel 40 to 188 in the target-full spectrum to the total number in the same interval in the target-empty spectrum. Defined in this way, the scale factor is 68 226/11 212$=6.09\pm0.06$; thus, in the region of the suspected peak, the statistical uncertainty in the zero level is $\sim\pm2$ counts. This amount of variation of the zero line has a negligible effect on the values of $\chi^2$ given in Table II. This statistical argument, however, rests entirely upon the assumption that the target-empty spectrum is the appropriate background. The only difference between the two spectra being subtracted is the presence or absence of liquid helium in the target vessel, and this is the basis for expecting that a deviation above the zero line is a signal from kaonic helium (the evidence that kaons were stopping in the liquid helium will be discussed in the next section). On the other hand, it can be argued that the helium itself can introduce a coincident background, by causing additional scattering and nuclear interactions of the kaons, for example. It would be remarkable, however, if this effect would produce a peak in the difference spectrum of the same width as an x-ray line.

If the zero level in the difference spectrum is assumed to be fixed by the above procedure, then the total number of counts in the interval from channel 143 to 174 is $540\pm205$, or 2.6 standard deviations above zero. The statistical center of this peak was located, in the same manner as the center of the $L_\alpha$ peak, at channel $(157.8\pm2.6)$, giving an energy value of $(35.4\pm0.9)$ keV. The Klein-Gordon value for the energy of the $K_\alpha$ line, corrected for nuclear size and vacuum polarization, is 34.9 keV.[16] The contributions to the quoted error (again, added in quadrature) are: 0.54-keV statistical uncertainty, 0.68-keV uncertainty in gain, 0.31-keV uncertainty in base line, and 0.11-keV uncertainty in linearity. The normal curve fitted to this peak by the method of least squares gave a full width at half maximum of $14.5_{-5.6}^{+6.2}$ channels, compared with an expected width of about 16 channels. The expected width includes an expected instrumental width of 14.9 channels broadened by an average gain drift during the individual runs of about 7 channels, added in quadrature. The least-squares fit of the normal curve also gave values for the center of the peak and the area under the peak consistent with the values quoted above.

To summarize the results of this section, it can be stated that the evidence for kaonic x rays is found in the difference spectrum, Fig. 4(b). This spectrum has a pronounced peak which corresponds to an energy consistent with the $L_\alpha$ transition. There is also some evidence for a second peak believed to be the $K_\alpha$ line. There is no evidence for the presence of the $L_\beta$ transition at 8.7 keV, or the $K_\beta$ transition at 41.3 keV, at intensities comparable to that of the $K_\alpha$. The $M_\alpha$ transition at 2.3 keV was not seen because of its low energy; it was too highly absorbed in the target to be detected. The main features of the data are the following.

(a) *Energy.* The energy values of the two lines were found to be: $6.5\pm0.4$ keV, assumed to be the $L_\alpha$ transition, and $35.4\pm0.9$ keV, assumed to be the $K_\alpha$ transition. Both of these energies are consistent with the Klein-Gordon values for kaonic helium, corrected for nuclear size and vacuum polarization[16]: 6.5 keV for the $L_\alpha$ line, and 34.9 keV for the $K_\alpha$. Assuming that the line identified as the $K_\alpha$ is real, this implies that the strong interaction contribution to the energy shift of the $1S$ level is $<1.0$ keV.

(b) *Linewidth.* The peaks were both fitted with normal curves to determine their widths, and both were consistent with the instrumental resolution width. The one standard deviation limit to the line broadening for the $K_\alpha$ transition is $<1.3$ keV. This corresponds to an upper limit on the rate of nuclear capture from the $1S$ state of $<2\times10^{18}$ sec$^{-1}$.

(c) *Intensity.* The total number of events in the $L_\alpha$ peak was found to be $1975\pm465$, and the total number in the peak believed to be the $K_\alpha$ was $540\pm205$. In order to compare intensities of the two lines, the efficiency for detection was calculated for each of the two energies. This was done by graphically dividing the target into 64 units of equal volume, and obtaining the efficiency for each small unit of volume by computing for each energy the absorption loss in the helium and in the walls of the target, the effective solid angle of the detector, and the absorption probability in the detector. The efficiency for each energy was then averaged uniformly over the volume of the target (the evidence that $K^-$ were stopping uniformly over the target volume will be discussed in the next section). The uncertainty in this calculation was estimated to be about $\pm5\%$. The detection efficiency values are 0.0205 for 6.5 keV, and 0.0114 for 34.9 keV; thus, the total number of x rays emitted during the experiment was: 96 300$\pm$23 100 $L_\alpha$ transitions, and 47 400$\pm$18 100 $K_\alpha$ transitions, and the ratio of $K_\alpha$ to $L_\alpha$ transitions is $0.49\pm0.22$. The absolute yield depends on a measurement of the number of $K^-$ stopped in the experiment. This is discussed in the following section.

[16] Y. Eisenberg and D. Kessler, Phys. Rev. 130, 2352 (1963).

## III. ABSOLUTE YIELD MEASUREMENT

The absolute yield of a transition is defined as the number of x rays per stopped meson. The absolute yield values for the transitions observed in this experiment are of interest in clarifying the picture of the nuclear capture of $K^-$ from atomic orbitals around the $\alpha$ particle. Specifically, the number of $K^-$ making the $L_\alpha$, or $n=3$ to $n=2$, transition shows directly the amount of nuclear capture from the higher atomic levels. A discussion of what can be deduced about the capture schedule from these results is given in Sec. IV.

Once the number of x rays has been found (previous section), the missing factor needed to determine the absolute yields is the number of $K^-$ stopped. The measurement of this number was not trivial because the beam was unseparated: although the stopping $K^-$ signal, $C_1C_2D$, was used as a gate for the observation of the x rays, it was too highly contaminated to give an accurate measure of $K^-$ stopping in the target. The measurement was performed by placing $C_1C_2D$ in coincidence with a detector system, $N$ in Fig. 2, which responded to secondaries from the target at approximately 90° to the beam. This signal was observed to be strongly dependent on the secondaries from $K^-$ interacting at rest in the target, and was used to calculate the number of $K^-$ stopping.

The detector system, $N$, viewing secondaries from the target consisted of three large NaI(Tl) crystals embedded in heavy lead shielding. The crystals were 10.2 cm thick by 22.9 cm in diameter, and subtended a solid angle of 4.8% of the total sphere. The threshold of the system was set to be just below the pulses given by minimum-ionizing cosmic-ray muons going directly through the 10.2-cm thickness. This threshold corresponded to an energy loss in the crystal of 49±5 MeV; the error quoted is an estimate of the uncertainty in the threshold adjustment. A fast-logic pulse was derived from the leading edge of the NaI pulse and was used to form the coincidence $C_1C_2DN$.

In order to verify that this signal was caused by $K^-$ stopping in the helium target, it was observed as a function of beam momentum around 840 MeV/$c$. The result of this observation is shown in Fig. 5. The signal is seen to drop for lower momenta, where the $K^-$ stop in the degrader before reaching the target, and again for higher momenta, as the range of the kaons exceeds that of the degrader plus target. The width of this peak (±1.9%) is consistent with the momentum acceptance of the beam broadened by range fluctuation. The uncertainties shown are those of counting statistics. Accidental rates were monitored, using delayed coincidence, and corrected for: they were typically less than 20% of the signal. This measurement was made immediately after the x-ray run, and the vertical scale has been normalized to the same beam monitor $\Gamma$ that was used to monitor the x-ray run.

A range curve can be deduced from Fig. 5 by substituting for the momentum value of each point, the thickness of copper required to stop $K^-$ of that momentum. When this was done, the peak was found to have a full width at half maximum of about 25 g/cm². Since the helium target thickness was only 4 g/cm², this would imply that the $K^-$ were stopping uniformly along the length of the target. In the plane perpendicular to the beam direction, the $K^-$ could be expected to stop uniformly over the target because of multiple scattering in the degrader. As an experimental check of this, the counts from the coincidence of $C_1C_2D$ with each of the three different NaI detectors (each was in the plane perpendicular to the beam direction, and each was separated by 45° in that plane) were found to be equal at 840 MeV/$c$, within a statistical uncertainty of about 12%.

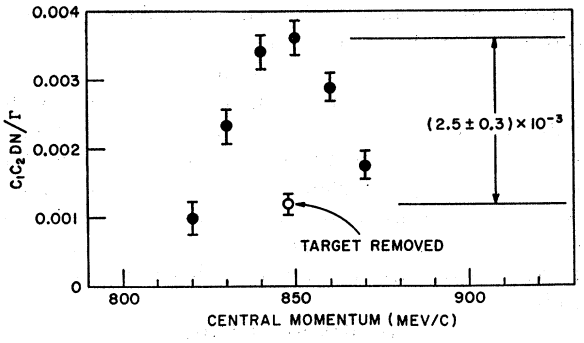


FIG. 5. The stopping $K^-$ signal as a function of beam momentum. The counters $C_1$, $C_2$, $D$, and $N$ are shown in Fig. 2. $\Gamma$ was the beam monitor.

The rate shown in Fig. 5 with the target removed is a direct measurement of the amount of background in this signal, and subtracting it from the peak value gives a number dependent only on $K^-$ interacting at rest in the helium. The number of $K^-$ stopped in the experiment, then, is given by

$$N_{K^-}=\Gamma S/\mathcal{E},$$

where

$\Gamma$ = monitor counts during x-ray run $=2.871\times10^6$,

$$S=\left(\frac{C_1C_2DN}{\Gamma}\right)_{\text{target full}}-\left(\frac{C_1C_2DN}{\Gamma}\right)_{\text{target removed}}$$

$$=(2.5\pm0.3)\times10^{-3},$$

$\mathcal{E}$ = efficiency of $C_1C_2DN$ for stopping $K^-$.

The efficiency $\mathcal{E}$ was calculated in the following three steps. (1) The observed branching ratios for all possible $K^-$ interactions at rest in helium were obtained from helium bubble chamber measurements.[17] (2) The energy distributions of all of the secondaries produced in the

[17] Helium Bubble Chamber Collaboration Group, in *Proceedings of the 1960 International Conference on High Energy Physics at Rochester* (Interscience Publishers, Inc., New York, 1960), pp. 423 and 426; also J. B. Kopelman (private communication).

various interactions, and their probability for intercepting the NaI crystals were computed by the Monte-Carlo method. (3) The detection probability for each type of secondary was computed from its energy distribution. This could be done using the known properties of energy loss of the secondary particles in NaI, since the energy threshold of the crystals was known. A detailed description of the calculation of $\mathcal{E}$ and a discussion of the estimated uncertainty in this calculation is given in the Appendix. The efficiency was computed to be

$$\mathcal{E}=0.0630\pm0.0076,$$

where the error quoted is the estimated uncertainty in the calculation.

Using this value for $\mathcal{E}$, the number of $K^-$ stopped in the x-ray experiment becomes $N_{K^-}=114\,000\pm19\,000$. Taking the number of x rays in each transition from the previous section, we obtain the following numbers for the absolute yields:

$$\text{yield of } L_\alpha \text{ transition}=0.85\pm0.25,$$
$$\text{yield of } K_\alpha \text{ transition}=0.42\pm0.17.$$

## IV. ATOMIC CASCADE AND NUCLEAR ABSORPTION

The high yield for the $L_\alpha$ transition measured in this experiment shows directly that the amount of nuclear absorption from states with $n\geqslant 3$ is small; in fact, it is $\lesssim 15\%$. It is useful at this point to investigate the atomic cascade, to construct a model which gives the observed high $L_\alpha$ yield, and to use this model to predict quantitatively the complete nuclear capture schedule for kaons in liquid helium. As a further constraint, the model must predict an average cascade time consistent with the observed value of $(2.4\pm0.4)\times10^{-10}$ sec.[4]

The capture schedule for kaons and pions in liquid *hydrogen* has been discussed in the literature for several years; it was first investigated by Wightman[18]; later extended by Day, Snow, and Sucher,[9] and by Russell and Shaw[10]; and most recently worked out in detail by Leon and Bethe.[11] The result is that the rate for Stark mixing of the angular-momentum states is sufficiently high to lead to rapid nuclear capture from the higher levels: $n\geqslant 3$ for pions, and $n\geqslant 5$ for kaons. This conclusion is re-enforced by the fact that the calculation successfully predicts the short ($\sim2\times10^{-12}$ sec) cascade times which have been observed.[6-8]

The situation has been less clear for liquid *helium*, however. A theoretical investigation of the capture process in helium was initially given by Day,[19] who concluded that Stark mixing induced by molecular fields would be sufficient to lead to rapid $S$-state capture from the higher levels, and predicted a capture rate similar to that for hydrogen. Later, the cascade times were measured[3,4] and found to be longer by a factor of about 100. In order to understand these results, another theoretical investigation was undertaken by Russell,[5] who made new estimates of the rates for de-excitation and obtained times about five times shorter than the observed values. He regarded this factor to be consistent with the approximations used in his calculations. He also made estimates of the rates for nuclear capture from higher levels caused by molecular-field Stark mixing and obtained rates comparable to the rates for de-excitation; however, the uncertainty in these calculations made it impossible to determine conclusively the amount of capture from higher levels. Another model for the capture process has recently been proposed by Condo.[20] He suggested that most mesons are rapidly captured from the higher levels as predicted by Day, but that the (apparently) long cascade times measured result from the decay of a small population of the mesons that form metastable atomic states.

The x-ray yields measured in the present experiment settle this question empirically: $\approx85\%$ of the kaons survive nuclear capture down to $n=2$. This provides a direct guide to a theory of the atomic cascade and nuclear-capture schedule. Since the survival of kaons down to $n=2$ is so large, we are led to consider a model for the cascade in which the rates for de-excitation from the higher levels are much larger than the rates for nuclear capture induced by molecular-field Stark mixing in these levels. In the remainder of this section, we describe a calculation of the atomic cascade and nuclear capture schedule based on this simple model. This calculation is similar to calculations done by Eisenberg and Kessler for muons,[21] pions,[22] and kaons,[16] in elements with $Z\geqslant 3$. In kaonic helium, the de-excitation is dominated by the external Auger effect in the higher levels and by radiation in the lower levels. In the calculations of Eisenberg and Kessler, the de-excitation is dominated in the higher levels by the *internal* Auger effect, but the matrix elements for the external Auger transitions are similar. After computing the $E1$ matrix elements for the external Auger and radiative de-excitation, a Monte-Carlo calculation was made of the atomic cascade, starting from an initial level in the neighborhood of $n=24$, with an assumed initial population of the angular momentum states. This calculation gave predictions for the mean time spent in the atomic cascade, the yields of the lowest x-ray transitions, and the nuclear-capture schedule.

One particularly interesting feature was encountered in this calculation of the cascade: A model which completely neglects Stark mixing predicts that in the higher levels, the states with maximum angular momentum will be metastable with respect to de-excitation. Above $n=16$, the spacing between the adjacent energy levels of kaonic helium is less than the ionization potential of

[18] A. S. Wightman, Ph.D. thesis, Princeton University, 1949 (unpublished); Phys. Rev. **77**, 521 (1950).
[19] T. B. Day, Nuovo Cimento **18**, 381 (1960).
[20] G. T. Condo, Phys. Letters **9**, 65 (1964).
[21] Y. Eisenberg and D. Kessler, Nuovo Cimento **19**, 1195 (1961).
[22] Y. Eisenberg and D. Kessler, Phys. Rev. **123**, 1472 (1961).

atomic helium, and no external Auger transitions can occur for $\Delta n=-1$. Since the states with maximum $l$ can make only a $\Delta n=-1$ transition in the $E1$ approximation, and since the radiative rates are low for these transitions, these states must be metastable on the time scale of the atomic cascade. We are thus led to the conclusion that although the rate for Stark mixing in the higher levels was assumed to be low enough to prevent much nuclear capture from $S$ states, it must nevertheless be high enough to depopulate these states rapidly. A more quantitative estimate of this is made later in this section.

### A. Description of the Cascade

Before proceeding to details of the cascade calculation, it may be helpful to review the general description of the atomic cascade and nuclear capture for kaonic helium. Although quantitative calculations of absolute rates have been uncertain, the general physical picture of the competing mechanisms involved in the cascade is well understood.[4,5] After losing energy by ionization and excitation, the free kaon rapidly displaces two electrons from a helium atom and finds itself bound in an atomic orbital around the alpha particle,[23] with a binding energy roughly equal to the ionization potential of the two electrons; this corresponds to $n\approx 24$. The atomic cascade, then, begins from principal levels in the neighborhood of $n=24$, and the system de-excites until the kaon is captured by the nucleus. Nuclear capture occurs from states in which the kaonic wave function has a large overlap with the nucleus; i.e., from $S$ states, and possibly from $P$ states. The de-excitation occurs in the higher levels by the ejection of electrons from neighboring helium atoms during collisions (external Auger effect). The partial rates for the external Auger transitions are largest for the smallest possible change in $n$; therefore, the de-excitation proceeds from the higher levels in small steps of $n$, with $\Delta l=\pm 1$. For levels below $n\approx 5$, the rate for radiation becomes large compared with the rate for external Auger transitions, and the de-excitation proceeds exclusively by radiative transitions.

Stark mixing of the angular-momentum states within a principal level is induced by the electric fields acting on the $K\alpha^+$ system during collisions. The high rate of Stark mixing in hydrogen is caused by the fact that the $Kp$ mesonic atom is a neutral object which can freely penetrate the electronic cloud during a collision and experience the strong electric field in the neighborhood of the nucleus. In helium, the $K\alpha^+$ system is a charged object which is repelled from the region of strong electric field near the nucleus; however, it does experience molecular fields during collisions which may lead to substantial rates for Stark mixing.[5,19]

[23] The time taken for the kaon to reach this state is usually referred to as the *moderation* time, while the *cascade* time is defined as the time spent in bound atomic states before nuclear capture. The mean time measured in bubble chamber experiments is the sum of these two; however, for liquid helium, the moderation time is short compared with the cascade time, so the experimental time is loosely referred to throughout this discussion as the cascade time

### B. Calculation of the Rates

The first thing needed for the cascade calculation was a computation of the de-excitation rates. Given each state, the rate was calculated for external Auger and radiative transitions to each allowed lower state. These partial rates were summed to give the total rate of decay from the state, and normalized to the total rate to give the branching ratio for each allowed transition. In the Monte-Carlo calculation of the atomic cascade, this information was stored in matrices, and used to provide the appropriate statistical weights for the transitions and for the time spent in each state.

A more detailed description of the calculation of the de-excitation rate follows. Throughout this paper, all relations will be expressed in atomic units ($a_0=m_e=e^2=\hbar=\alpha c=1$), unless specifically designated otherwise.

The total rate of decay from a state, characterized by $(n,l)$, is given by

$$\Gamma_{nl}=\Gamma_{nl}(\text{radiative})+\Gamma_{nl}(\text{Auger})$$
$$\sum_{n'l'}\Gamma_{nl}{}^{n'l'}(\text{radiative})+\sum_{n'l'}\Gamma_{nl}{}^{n'l'}(\text{Auger}), \quad (1)$$

where the summation extends over all final states $(n',l')$ allowed by $E1$ transitions. Higher-order multipoles are ignored, of course, since their rates are negligible in comparison. The branching ratio for each transition is simply

$$B_{nl}{}^{n'l'}=[\Gamma_{nl}{}^{n'l'}(\text{rad})+\Gamma_{nl}{}^{n'l'}(\text{Aug})]/\Gamma_{nl}. \quad (2)$$

The radiative rates are well known; they are given by[24]

$$\Gamma_{nl}{}^{n'l'}(\text{rad})=\Gamma_R\left(\frac{1}{n'^2}-\frac{1}{n^2}\right)^3\left(\frac{l+s}{2l+1}\right)(R_{nl}{}^{n'l'})^2, \quad (3)$$

$$\Gamma_R=\tfrac{1}{6}\alpha^3Z^4M_K$$
$$=Z^4M_K(2.675\times 10^9)\ \text{sec}^{-1},$$

where $Z$ is the nuclear charge, and $M_K=m_Km_\alpha/(m_K+m_\alpha)$, the reduced mesonic mass (853.5 for kaonic helium). The $E1$ selection rules are given by

$$l=l'\pm 1,$$
$$s=1, \quad \text{for} \quad l'=l+1$$
$$=0, \quad \text{for} \quad l'=l-1.$$

The hydrogenic dipole matrix element, $R_{nl}{}^{n'l'}$, is

[24] H. A. Bethe and E. E. Salpeter, *Quantum Mechanics of One- and Two-Electron Atoms* (Academic Press Inc., New York, 1957), Chap. IV.

given by[25]

$$R_{nl}{}^{n'l'}=\int_0^\infty R_{n'l'}(r)R_{nl}(r)r^3dr\,, \tag{4}$$

where $R_{nl}(r)$ is the hydrogenic radial wave function.

The external Auger rate is more difficult to calculate with certainty. Leon and Bethe[11] have calculated this rate in liquid hydrogen in the Born approximation, using plane waves for the relative motion, and Coulomb wave functions for the ejected electrons. Although the validity of this calculation is much less certain for liquid helium, it has been used here to obtain the rates for the cascade calculation. The relative velocity in collisions is about the same for the mesonic atom in helium as in hydrogen (after the first external Auger transition, the charged $K\alpha^+$ must recoil from the $He^+$ ion with a few eV of kinetic energy), so as a first guess, the Born approximation appears still to be valid. What has been ignored, however, is the fact that the charged $K\alpha^+$ adiabatically distorts the electronic wave functions around the helium atom during a collision. If this effect is important, it should tend to increase the rates (since it would tend to increase the density of the bound electrons in the neighborhood of the $K\alpha^+$) from the values calculated with the undistorted wave functions. In any case, the ultimate justification of this method is the fact that the results of the cascade calculation are relatively insensitive to the absolute value of the Auger rate. This was investigated by multiplying the values of $\Gamma_{nl}{}^{n'l'}(\text{Aug})$ obtained by this method by a common strength factor before combining them with the radiative rates in Eqs. (1) and (2). The absolute yields of the lowest x-ray transitions given by the cascade calculation were then observed as this factor was varied from 0.1 to 10. When the strength factor was varied over this wide range, the absolute yields were found to change by only $\pm 4\%$; thus, this method for calculating the external Auger rates seems to be appropriate for the present discussion.

Taking the calculation of Leon and Bethe over for helium, then, leads to the following expression for the external Auger de-excitation rate:

$$\Gamma_{nl}{}^{n'l'}(\text{Aug})=\Gamma_A I(k)\left(\frac{l+s}{2l+1}\right)(R_{nl}{}^{n'l'})^2 \tag{5}$$

$$\Gamma_A=\frac{16\pi}{3}\frac{N_e[1+(Z-1)\epsilon]^2}{Z_e Z^2 M_K}$$

$$=(1.028\times10^{-7})\times N(\text{in cm}^{-3})\times\frac{[1+(Z-1)\epsilon]^2}{Z_e Z M_K}\text{sec}^{-1},$$

where $Z_e$ is the effective charge on a bound electron (1.69 for helium), $\epsilon=m_K/(m_K+m_\alpha)=0.117$ for kaonic helium, and $N_e$ is the density of electrons ($=Z\times$atomic density). The density of liquid helium, $N$, used in the calculations was $1.884\times10^{22}$ cm$^{-3}$.

[25] This definition is the same as that found in Ref. 24, p. 264.

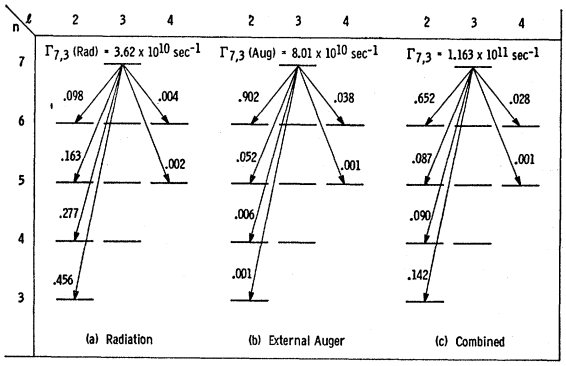


FIG. 6. De-excitation branching ratios for the state, $(n,l)=(7,3)$. For this example, the radiative and external Auger rates are comparable in magnitude.

The selection rule for $l$ is the same as for radiation; however, the $\Delta n$ dependence is quite different. It is given by the function $I(k)$, where $k$ is the (asymptotic) wave number of the ejected Auger electron. Over the range of $k$ needed for these calculations, this function can be approximated to a few tenths of a percent by[26]

$$I(k)\approx(k^2/Z_e{}^2+1.39)^{-1/2}. \tag{6}$$

The wave number $k$ is fixed for a given transition by conservation of energy. Since the $K\alpha^+$ is much more massive and moves slower than the ejected electron, any change in relative motion during the transitions may be neglected, and

$$k^2=Z^2M_K\left(\frac{1}{n'^2}-\frac{1}{n^2}\right)-2\delta\,, \tag{7}$$

where the first term is simply (twice) the energy lost by the $K\alpha^+$ system in the transition, and $\delta$ is the ionization energy for the electron ($2\delta=1.807$, for helium).

The external Auger transitions, then, are most probable for the smallest possible change in $n$, whereas the radiative transitions favor the largest possible change in $n$. This situation is illustrated in Fig. 6(a) and 6(b), where the branching ratios for radiative and external Auger transitions are given separately for the state $(n,l)=(7,3)$. For this state, the Auger rates are comparable with the radiative rates, and the combined effect is shown in Fig. 6(c). For higher levels, the Auger rate dominates, and the de-excitation proceeds mostly in small steps.

A direct comparison of the calculated external Auger de-excitation rates, $\Gamma_{nl}(\text{Aug})$, to the radiative rates, $\Gamma_{nl}(\text{rad})$, is shown in Fig. 7, where these rates have been

[26] Leon and Bethe have given this approximation for $I(k)$ in Ref. 11. It can be evaluated by numerical integration. This was done for several values of $k$ over the range of interest, and compared with the approximation to establish the accuracy quoted here.

plotted as a function of $n$, for various $l \leqslant 5$. The dominance of radiation in the lower levels and the dominance of external Auger transitions in the higher levels can clearly be seen.

For $n \geqslant 17$, the energy difference between the adjacent kaonic levels is less than the ionization potential of helium, and it becomes impossible to eject Auger electrons for $\Delta n = -1$; i.e., in Eq. (7), $k^2 < 0$, for $n' = n-1$. For these cases, the smallest possible value of $-\Delta n$ consistent with $k^2 \geqslant 0$ is preferred. This raises another important question which must be dealt with in the cascade calculation: how are states with maximum $l$ depopulated when $n \geqslant 17$?

Consider the example illustrated in Fig. 8. A transition from the state $(n,l) = (17,16)$ is energetically forbidden for the ($E1$) external Auger process. Radiation is allowed, but its decay time ($\sim 10^{-8}$ sec) is much longer than the time observed for the entire cascade. This suggests that the rate for Stark mixing with the adjacent state (17,15) is sufficient to induce depopulation through the allowed external Auger transition from (17,15) to (15,14).

This view is not inconsistent with the model under consideration: the model has assumed that the rate for *nuclear capture* via Stark mixing is negligible compared with the rate for de-excitation. The rate for Stark mixing between states with *adjacent $l$ values* is likely to be much higher. An estimate of the frequency for Stark oscillations between such states can be made by

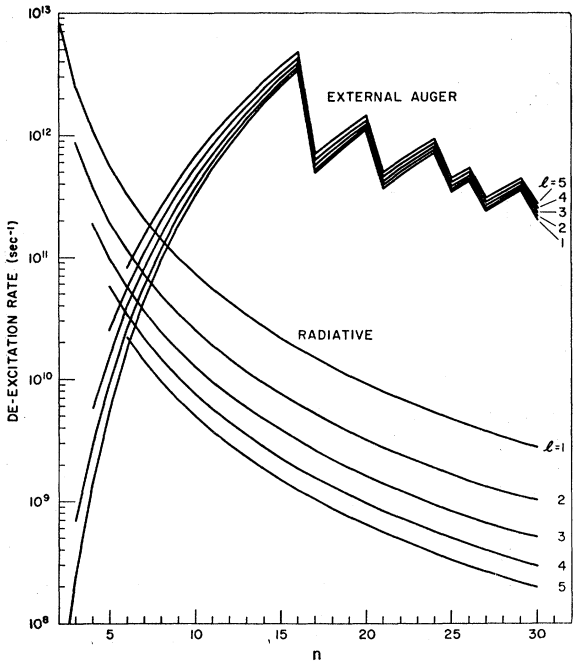


FIG. 7. De-excitation rates for radiative and external Auger transitions in kaonic helium for $l \leqslant 5$.

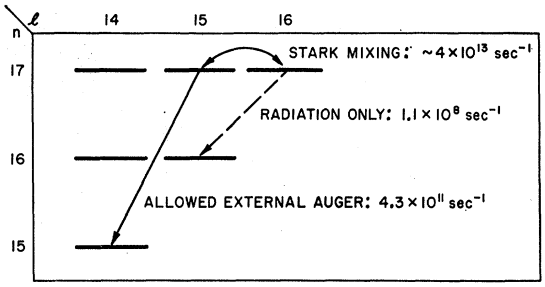


FIG. 8. Depopulation of the state $(n,l) = (17,16)$. External Auger is energetically forbidden; radiation is possible, but the rate is low. Stark mixing induces the allowed transition through (17,15) to (15,14).

estimating the following matrix element[11]:

$$\omega_{\text{Stark}} = \langle n,l-1 \,|\, \boldsymbol{F}\cdot\mathbf{r} \,|\, n,l \rangle$$
$$\approx F_{\text{av}} \frac{1}{M_K} R_{nl}{}^{nl-1} \tag{8}$$
$$\approx n(2n-1)^{1/2} F_{\text{av}}/M_K, \quad \text{for} \quad l = n-1.$$

If the average molecular electric field during a collision, $F_{\text{av}}$, is taken to be $\sim 0.01$,[5] the rate for Stark mixing between $(n,l) = (17,16)$ and (17,15) is $\sim 4\times 10^{13}$ sec$^{-1}$. The two states, then, are rapidly mixed, and depopulation occurs by means of the allowed external Auger transition from (17,15).

This example illustrates the other major assumption used in the cascade model: all states from which Auger transitions are energetically forbidden ($n \geqslant 17$, $l \approx$ maximum) are depopulated by rapid (instantaneous) Stark mixing with the nearest state within the principal level from which an external Auger transition is allowed. This assumption appears reasonable in light of the above estimate.

The remaining numbers needed for the cascade calculation are the rates for nuclear capture. Capture from $S$ states was assumed to be instantaneous compared with the time scale of the de-excitation process.[27] The rate for $P$ capture could be varied in the calculation, allowing the possibility of either de-excitation or capture from $P$ states on the way down. It has been previouslv pointed out, in Ref. 1, that the ratio of intensities, $K_\alpha/L_\alpha$, gives a direct measure of the rate of capture from the $2P$ level. In the present case, the $2P$ capture rate was found by using it as an input to the calculation, and adjusting it until the observed $K_\alpha/L_\alpha$ intensity ratio was obtained. The rates of capture from the $nP$ states were computed by assuming that they were proportional to the amount of overlap of the square of

[27] The capture rate from $S$ states has been estimated by Day in Ref. 19 to be $\sim(2\times 10^{19})/n^3$ sec$^{-1}$, from the $\bar{K}$-nucleon scattering lengths, assuming simple additivity in helium. This assumption may not be valid (Sec. V of the present paper); however, the $S$-state capture rate could be reduced by several orders of magnitude and still be instantaneous on the time scale of the de-excitation.

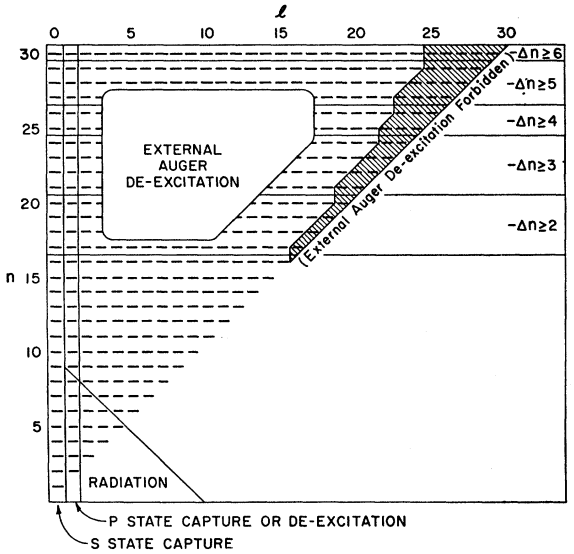


FIG. 9. Diagram of the atomic states, showing the processes involved in the atomic cascade of kaonic helium. The diagonal line indicates the boundary between the states in which radiative, and external Auger transitions, respectively, dominate the de-excitation. To the right, the minimum change in $n$ required for external Auger transitions is listed, and the resulting states from which external Auger transitions are forbidden are shown in the shaded region.

the kaonic wave function with the nucleus to first order; this gives

$$\Gamma_{nP}=\frac{32}{3}\frac{1}{n^3}\left(1-\frac{1}{n^2}\right)\Gamma_{2P}. \tag{9}$$

### C. Calculation of the Cascade

A diagram of the atomic states with $n\leqslant 30$ is given in Fig. 9. The various features of the model used to calculate the cascade for kaonic helium are shown on the diagram. The diagonal line indicates the division between the lower states, in which radiation dominates the de-excitation, and the higher states, in which external Auger transitions dominate. For the higher states, $n\geqslant 17$, the minimum change in $n$ for which external Auger transitions are allowed is listed and the resulting high-$l$ states from which external Auger transitions are forbidden are indicated in the shaded area of the diagram.

TABLE III. Results of the atomic-cascade calculation, expressed as a function of $n$, the initial principal level from which the cascade began. The initial $l$ distribution was $\sim(2l+1)e^{0.2l}$ (see text). For $n=24$, the binding energy of kaonic helium equals the ionization potential (for the two electrons) of atomic helium.

| $n$ | $L_\alpha$ yield | Mean cascade time ($10^{-10}$ sec) |
|---|---|---|
| 22 | 0.85 | 0.4 |
| 23 | 0.86 | 0.4 |
| 24 | 0.89 | 0.5 |
| 25 | 0.91 | 0.8 |
| 26 | 0.93 | 0.8 |
| 27 | 0.94 | 1.9 |
| 28 | 0.95 | 1.9 |
| 29 | 0.96 | 1.9 |
| 30 | 0.96 | 5.4 |
| Observed values: | 0.85±.25[a] | 2.4±0.4[b] |

[a] From this experiment.
[b] From Ref. 4.

The (Monte Carlo) calculation of the cascade was performed in the following manner. First, the de-excitation rates, $\Gamma_{nl}$, and the de-excitation branching ratios, $B_{nl}{}^{n'l'}$, were calculated according to Eqs. (1) and (2), and stored in an array. Then, the cascade was started from a designated $n$-level and the initial $l$ was chosen from an initial $l$ distribution which could be varied. For each event, the cascade would proceed until capture occurred from a $P$ or $S$ state. For each transition in the cascade, the time spent in the state $(n,l)$ was generated from the distribution, $\exp(-\Gamma_{nl}t)$, and the new state was chosen according to the statistical weights given by $B_{nl}{}^{n'l'}$. After generating the desired number of cascades, the following results were presented: the number

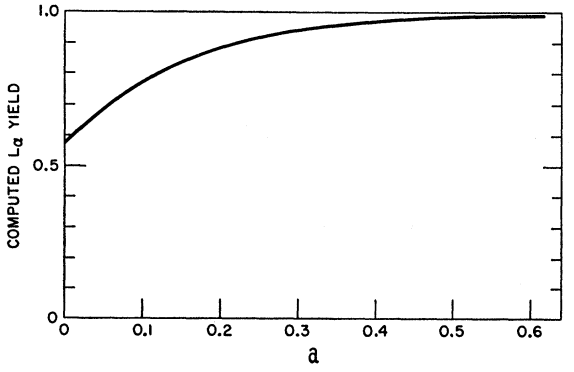


FIG. 10. Computed $L_\alpha$ yield as a function of $a$ in the initial $l$ distribution, $\sim(2l+1)\exp(al)$. The cascade was started at the $n=24$ level.

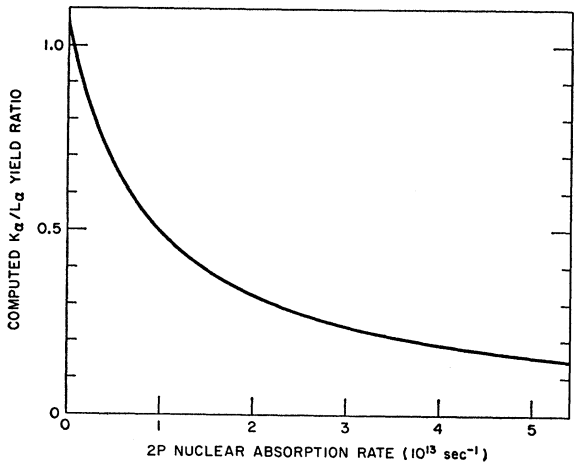


FIG. 11. Computed $K_\alpha/L_\alpha$ yield ratio as a function of the rate for nuclear absorption from the $2P$ state, using the cascade model described in the text.

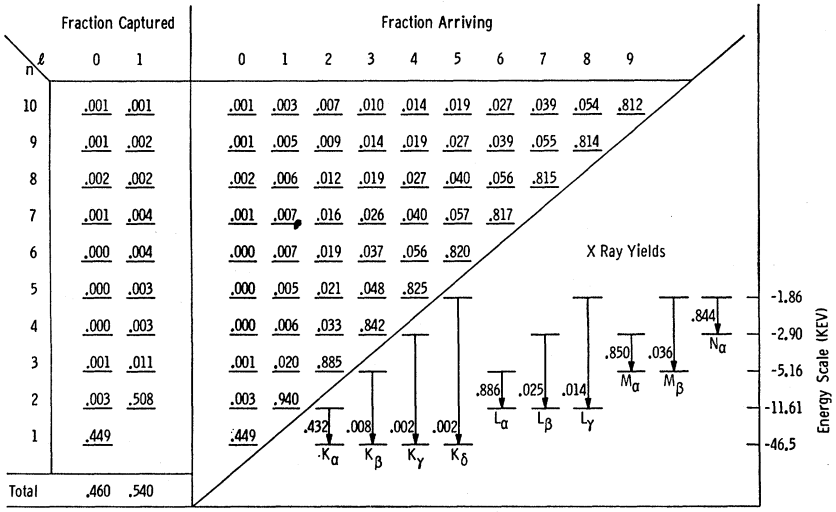


FIG. 12. Results of the calculation of the atomic cascade of kaonic helium. Shown are the fraction of kaons arriving at each atomic state below $n=10$, the fraction which undergo nuclear capture from $S$ and $P$ states, and the absolute yields of the x-ray transitions between the lower states. For this calculation, the cascade was started at $n=24$, with an initial $l$ distribution $\sim(2l+1)\times\exp(0.2l)$. All kaons reaching $S$ states were assumed captured, and the rates for $P$-state capture were computed assuming a $2P$ capture rate of $1.0\times10^{13}$ sec$^{-1}$ (see text).

arriving at each state $(n,l)$, the number captured from each $nP$ state (all reaching $S$ states were assumed captured), the absolute yield of each x-ray line below $n=4$, and the mean time for the cascade. The Monte Carlo method was used merely for convenience. The cascade routes and resulting capture schedules, of course, could have been computed directly, but the large number of states involved made the statistical method appear more attractive.

### D. Results of the Cascade Calculation

First, the starting level of the cascade was chosen to to be at $n=24$, and the initial $l$ distribution was chosen to be $\sim(2l+1)e^{al}$. This distribution provides for a greater population of the higher $l$ states than a purely statistical population, $\sim(2l+1)$. It has been taken from the calculations of Eisenberg and Kessler. They have successfully predicted the muonic[21] and pionic[22] x-ray yields observed in elements of higher $Z$ using this distribution with $a\approx0.2$. Since the present calculation is similar, we have used this initial distribution. As a check of the sensitivity of the results to this assumption, the cascade calculation was performed for several values of $a$, and the resulting $L_\alpha$ yield obtained as a function of $a$ is shown in Fig. 10. Almost any value of $a$ in the distribution gives an $L_\alpha$ yield consistent with the experimental yield of $0.85\pm0.25$, since the experimental uncertainty is large. Since the value $a=0.2$ has given good fits to the muonic and pionic yields in the calculations of Eisenberg and Kessler, we have adopted it for the subsequent calculations.

It was also of interest to study the results of the cascade calculation as a function of the starting level of the cascade; the results are listed in Table III. The $L_\alpha$ absolute yield is seen to be relatively insensitive to the assumed starting level. Near $n=24$, the cascade times given by the calculation tend to be somewhat lower than the observed value. This suggests that the mean starting level for the cascade is somewhat higher; say, $n=27$ to 30.[28] For the subsequent calculations, however, we have taken $n=24$ as the starting level, since the absolute yield is relatively insensitive to this choice.

The ratio of the $K_\alpha$ yield to the $L_\alpha$ yield given by the calculation depends sensitively on the strength of the nuclear absorption rate from $P$ states. The rate of absorption from the $2P$ state, $\Gamma_{2P}$, was used as an input to the cascade calculation (as described in the last paragraph of part B of this section), and the $K_\alpha/L_\alpha$ yield ratio was obtained as a function of $\Gamma_{2P}$; the result is given in Fig. 11. If we take (from Sec. II) the observed $K_\alpha/L_\alpha$ yield ratio, $0.49\pm0.22$, then we obtain from Fig. 11,

$$\Gamma_{2P}=(1.0_{-0.6}{}^{+1.5})\times10^{13}\ \text{sec}^{-1}.$$

This value, of course, is based on the assumption that the second peak in the observed spectrum is indeed the $K_\alpha$ transition and not a statistical fluctuation. If it is a large statistical fluctuation, then the above number should be taken as a lower limit. For the purpose of computing the capture schedule, the $2P$ absorption rate was assumed to be fixed at $1.0\times10^{13}$ sec$^{-1}$.

The final result of the cascade calculation is given in Fig. 12. The fraction surviving down to each level with $n\leqslant10$ is given, together with the resulting capture schedule and predicted yields of the lowest few x-ray transitions.

## V. CONCLUSIONS

The nuclear-capture schedule calculated in the previous section predicts that $\sim95\%$ of the kaons undergo nuclear absorption from atomic states with $n\leqslant2$, and that $\sim55\%$ of the absorption occurs from $P$ states and $\sim45\%$ occurs from $S$ states. The high fraction surviving absorption down to $n=2$ is well established since it is a

[28] Russell has stated a similar conclusion in Ref. 5.

direct consequence of the observed high $L_\alpha$ x-ray yield. The fraction of $P$-state absorption is less well established, since it depends on the intensity of the peak in the observed spectrum which has been interpreted to be the $K_\alpha$ line; however, if this peak is merely a statistical fluctuation and the $K_\alpha$ intensity is lower than estimated in Sec. II, the fraction of $P$-state capture would become still greater than that predicted above.

The capture schedule, then, conclusively shows that it is *not* possible to assume that all $K^-$ are captured from $S$ states in helium, as is the case for hydrogen. The assumption of $S$-state capture originally had been used in part to establish the spins of the ground states of the hyperfragments ${}_\Lambda H^4$ and ${}_\Lambda He^4$,[29] and the spin and parity of the $Y_1^*(1385)$[30,31]; however, in both of these cases, the quantities in question have since been determined by independent means.[32] The use of this assumption in a recent theoretical investigation of the reaction $K^-+He^4 \rightarrow \pi^-+\Lambda+He^3$ is worth mentioning. Said and Sawicki have calculated the momentum distributions of $\pi^-$ and $He^3$ from this reaction under the assumption that all $K^-$ are captured from $S$ states.[33] This calculation has recently been repeated assuming $P$-state capture.[34] There is little change in the $He^3$ distribution, but the $\pi^-$ distribution appears to be in better agreement with the experiment.

The fact that as high as 55% of the $K^-$ are captured from $P$ orbits makes the possibility of the formation of the $J=1$ excited states of the hyperfragments, ${}_\Lambda H^{4*}$ and ${}_\Lambda He^{4*}$, still an open question. Conservation of angular momentum requires that the capture must occur from $P$ levels in order to form these objects, but only the spin flip part of the $P$-wave interaction $\bar{K}+N \rightarrow \Lambda+\pi$, can form the $J=1$ final state of the hyperfragment. It is not presently known how much of the interaction can contribute to the spin flip.[35]

In spite of the fact that the evidence for the $K_\alpha$ peak is not overwhelming (Table II), it might be interesting to explore the consequences which follow if we assume that it is a real effect. The existence of this line leads to experimental information on three quantities which are related to the $\bar{K}$-$\alpha$ interaction: (1) from the measured energy of the $K_\alpha$ line, the upper limit on the $1S$ energy level shift was established to be $<1.0$ keV; (2) from the experimental upper limit to the broadening of the $K_\alpha$ line, the absorption rate from the $1S$ level was established to be $<2\times10^{18}$ sec$^{-1}$; and (3) from the intensity of the $K_\alpha$ line relative to the $L_\alpha$, together with a calculation of the atomic cascade, the absorption rate from the $2P$ level was established to be $(1.0_{-0.6}{}^{+1.5})\times10^{13}$ sec$^{-1}$.

The first two of these quantities can be interpreted as the real and imaginary part, respectively, of the complex energy level shift of the $1S$ level. This complex energy shift, $\Delta E_{1S}$, can be related to the $S$-wave complex scattering length for the $\bar{K}$-$\alpha$ system, $A$, by the relation[36–38]

$$\Delta E_{1S}=-4(A/a_0)E_{1S}, \tag{10}$$

where $a_0$ is the Bohr radius for the system (31.0 F), and $E_{1S}$ is the unperturbed energy of the $1S$ level ($-46.5$ keV). This relation is valid as long as $|A|\ll a_0$.[38] If we assume that the $\bar{K}$-$\alpha$ scattering length can be obtained by simple additivity of the $\bar{K}$-nucleon scattering lengths, we have $A=3A^1+A^0$, where $A^1$ and $A^0$ are the ($S$-wave) scattering lengths for the isotopic spin 1 and 0 channels, respectively. If we take[39] $A^0=(1.6+i0.5)$ F, and $A^1=(-0.2+i0.4)$ F, we obtain $\mathrm{Re}(\Delta E_{1S})=-13$ keV and $\mathrm{Im}(\Delta E_{1S})=1.7\times10^{19}$ sec$^{-1}$. Both of these predictions are about an order of magnitude larger than the corresponding experimental limits. The third experimental quantity listed above, the $2P$ absorption rate, can also be predicted using simple arguments. If we ignore the possibility of a nonlocal $\bar{K}$-$\alpha$ interaction, we can estimate the amount of the $2P$ absorption rate due to the $S$-wave part of the interaction by assuming that it is proportional to the amount that the square of the $P$ wave function overlaps the $\alpha$ particle. To first order, this gives for the absorption rate from the $nP$ state,

$$\Gamma_{nP}=\frac{1}{15}\left(1-\frac{1}{n^2}\right)\frac{1}{n^3}\left(\frac{r_\alpha}{a_0}\right)^2\Gamma_{1S},$$

where $r_\alpha$ is the radius of the $\alpha$ particle, and $\Gamma_{1S}$ is the $1S$ absorption rate. If we take the value for $\Gamma_{1S}$ given above by $\mathrm{Im}(\Delta E_{1S})$, and use $r_\alpha=1.7$ F,[40] we obtain $\Gamma_{2P}=3.2\times10^{14}$ sec$^{-1}$. This prediction also is about one order of magnitude larger than the corresponding experimental number.

There is, of course, no reason to believe that the assumption of simple additivity of the scattering lengths is appropriate for helium. The next most simple approach to try is to express the $\bar{K}$-nucleon interaction in terms of a complex potential, and to assume that the $\bar{K}$-$\alpha$

[29] M. M. Block, L. Lendinara, and L. Monari, in *Proceedings of the International Conference on High-Energy Physics, Geneva, 1962* (CERN Scientific Information Service, Geneva, Switzerland, 1962), p. 371.
[30] Helium Bubble Chamber Colloboration Group, Nuovo Cimento **20**, 724 (1961).
[31] J. Auman, M. M. Block, R. Gessaroli, J. B. Kopelman, S. Ratti, L. Grimellini, T. Kikuchi, L. Lendinara, L. Monari, and E. Harth, in *Proceedings of the International Conference on High-Energy Physics, Geneva, 1962* (CERN Scientific Information Service, Geneva, Switzerland, 1962), p. 330.
[32] M. M. Block, in Proceedings of the International Conference on Hyperfragments, St. Cergue, March, 1963, CERN Report 64/1, 1964 (unpublished), p. 63; also p. 75.
[33] P. Said and J. Sawicki, Phys. Rev. **139**, B991 (1965).
[34] J. Sawicki, Phys. Rev. **152**, 1246 (1966).
[35] R. H. Dalitz, "Hyponuclear Interactions," Clarendon Laboratory Report, Oxford, England, 1965 (unpublished).
[36] S. Deser, M. L. Goldberger, K. Baumann, and W. Thirring, Phys. Rev. **96**, 774 (1954).
[37] N. Beyers, Phys. Rev. **107**, 843 (1957).
[38] T. L. Trueman, Nucl. Phys. **26**, 57 (1961).
[39] M. Sakitt, T. B. Day, R. G. Glasser, N. Seeman, J. Friedman, W. E. Humphrey, and R. R. Ross, Phys. Rev. **139**, B719 (1965).
[40] G. R. Burleson and H. W. Kendall, Nucl. Phys. **19**, 68 (1960).

interaction can be expressed as a simple superposition of these potentials. This has been done in recent months in at least two different papers: Uretsky has used complex central square-well potentials,[41] and von Hippel and Douglas have used complex central Yukawa potentials.[42] The predictions of these two calculations are essentially in agreement. The $\bar{K}$-nucleon scattering lengths are used to fix the depth of the potentials, and the range remains as a free parameter. For ranges corresponding to any known particle exchange, these potentials predict a complex energy shift which is still about an order of magnitude larger than the experimental limits.

If we are to take these experimental numbers seriously, then, we are forced to the conclusion that either the $\bar{K}$-nucleon scattering lengths must be changed, or the $\bar{K}$-$\alpha$ interaction is not a simple superposition of the individual $\bar{K}$-nucleon interactions. It might be added that another, independent way to shed light on this problem would be to compute the complex-energy shift directly from the $\bar{K}$-$\alpha$ scattering length solutions and Eq. (10). To date, however, no measurements on low-energy $\bar{K}$-$\alpha$ scattering have been published.

## ACKNOWLEDGMENTS

The author is deeply indebted to Professor Robert A. Schluter for continued guidance throughout this work. The author is also grateful for the support of Professor Roger H. Hildebrand. It has been a pleasure to collaborate with the other members of the kaonic x-ray experimental group, particularly with Dr. George R. Burleson, Dr. Richard C. Lamb, and Dr. Thomas O. White, Jr., who have provided many stimulating discussions in extending this work. The author wishes also to acknowledge helpful discussions with Professor Arnold R. Bodmer, Professor Richard H. Dalitz, Professor Valentine L. Telegdi, and Dr. Jack L. Uretsky.

## APPENDIX. CALCULATION OF THE DETECTION EFFICIENCY OF THE STOPPING $K^-$ SIGNAL

In this Appendix, we describe the calculation of the detection efficiency of the signal, $C_1C_2DN$, used to measure the number of $K^-$ mesons stopped in the experiment. As described in Sec. III (see Fig. 2), the coincidence $C_1C_2D$ was a contaminated signal for slow $K^-$ entering the helium target, and $N$ was a system of three large NaI(Tl) crystals with a known energy threshold, which counted secondaries from $K^-$ interacting in the target. The problem, then, is to determine $\mathcal{E}$, the number of secondaries detected in $N$ per stopped $K^-$.

The first step was to find the branching ratios for all possible $K^-$ interactions at rest in helium, and to find the energy distributions of the products of these interactions. Final states for $K^-$+He at rest are listed in Table IV, and branching ratios observed in helium bubble-chamber data are given.[17] Also available from helium bubble-chamber measurements were the follow-spectra[17]: $\Lambda^0$ and $\pi^-$ from reaction 1, and $\Sigma^\pm$ and $\pi^\mp$ from reactions 3 and 5. The spectra of $\Sigma^0$ and $\pi^0$ from reaction 4 was assumed to be the same as $\Sigma^\pm$ and $\pi^\mp$ from 3 and 5, by charge symmetry. The spectra of $\Lambda^0$ and $\pi^0$ from reaction 2 was taken to be the same as those for $\Lambda^0$ and $\pi^-$ from reaction 1. This assumption cannot be justified by charge symmetry; however, this represented only 16% of the total interactions, and the final results were found to be insensitive to the choice of spectra in this channel. The hyperons in reactions 6 through 9 were assumed to be mono-energetic. This is a gross assumption, since the residual nucleons survive in a bound state in only a small fraction of the interactions; but again, these represent only 17% of the total and the final results were found to be insensitive to this choice. The reactions 10 through 14, representing only 5% of the total were ignored in the calculation. The residual nucleons, shown in parentheses in the table, were also ignored; they were generally of low energy and for the most part could not escape the target.

TABLE IV. Branching ratios for $K^-$ interactions at rest in helium used in the efficiency calculation.

| Final state | Observed number of events[a] | Percent of total events |
|---|---|---|
| 1. $\Lambda^0\pi^-$ $(ppn)$ | 363 | 33 |
| 2. $\Lambda^0\pi^0$ $(pnn)$ | 184 | 16 |
| 3. $\Sigma^+\pi^-$ $(pnn)$ | 136 | |
| 4. $\Sigma^0\pi^0$ $(pnn)$ | 110 | 29 |
| 5. $\Sigma^-\pi^+$ $(pnn)$ | 78 | |
| 6. $\Lambda^0$ $(pnn)$ | 62 | |
| 7. $\Sigma^+$ $(nnn)$ | 30 | 17 |
| 8. $\Sigma^0$ $(pnn)$ | 54 | |
| 9. $\Sigma^-$ $(ppn)$ | 42 | |
| 10. $\Lambda^0\pi^+$ $(nnn)$ | 21 | |
| 11. $\Sigma^0\pi^-$ $(ppn)$ | 18 | |
| 12. $\Sigma^-\pi^0$ $(ppn)$ | 14 | 5 |
| 13. $\Sigma^+\pi^0$ $(nnn)$ | 0 | |
| 14. $\Sigma^0\pi^+$ $(nnn)$ | 0 | |

[a] Reference 17.

The next step in the problem was to determine the energy distribution of the secondaries and their probability for intercepting the NaI crystals. This was done in a Monte-Carlo calculation.[43] For each event, the Monte-Carlo program proceeded in the following manner: (1) a location for the interaction was chosen from a uniform distribution over the volume of the target; (2) an interaction channel was selected accord-

[41] J. L. Uretsky, Phys. Rev. **147**, 906 (1966).
[42] F. von Hippel and J. H. Douglas, Phys. Rev. **146**, 1042 (1966).
[43] This calculation is similar to a background calculation for this experiment by G. R. Burleson and R. M. Schwarcz, Argonne National Laboratory Report No. GRB/RMS-1, 1963 (unpublished).

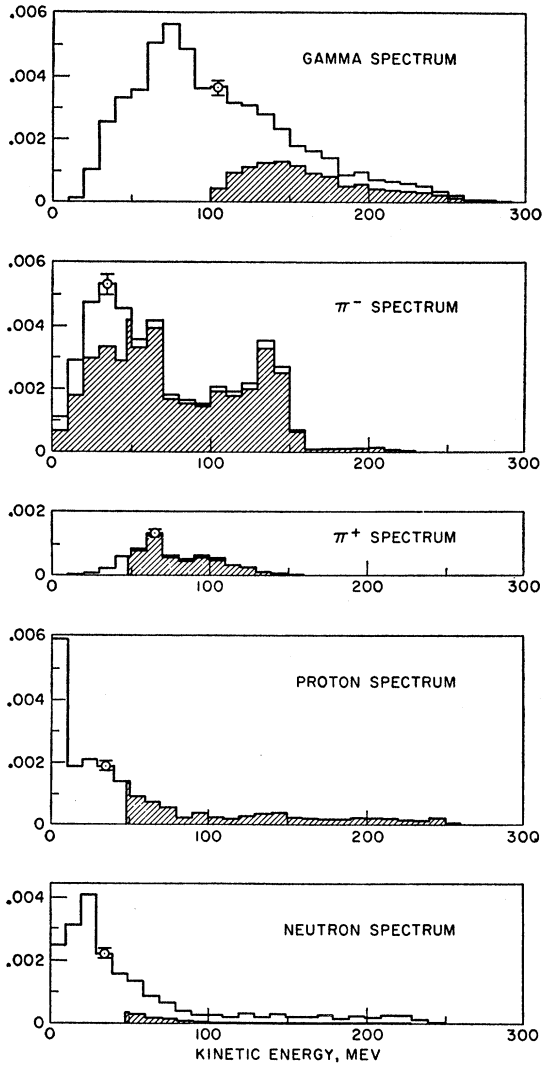


FIG. 13. Computed spectra of the secondaries from $K^-$ interactions at rest in helium. The vertical scale gives the number per stopped $K^-$. The unshaded spectra show the number of secondaries which pass through the NaI detector system, $N$, and the shaded portions show the number actually detected. The brackets indicate the amount of statistical uncertainty in the Monte-Carlo calculation.

ing to the branching ratios of Table IV; (3) the initial direction for each hyperon (and each pion) was selected from an isotropic distribution; (4) the energy of each hyperon (and each pion) was selected from the appropriate energy distribution; (5) a path length was selected for each hyperon from a distribution with the appropriate lifetime; (6) each hyperon (and each $\pi^0$) was decayed isotropically in its center of mass frame, and the energy, direction, and type of each secondary was determined in the laboratory frame; (7) from the direction of each secondary, it was determined whether or not it intercepted a NaI crystal; and (8) the energy and type of each secondary intercepting a crystal was recorded in a histogram. In this manner, a spectrum was computed for each type of secondary intercepting the detector system, $N$, and each spectrum was normalized to the number of stopping $K^-$. These spectra are given in Fig. 13. The spectra for the charged secondaries have been corrected for energy loss in the target.

The final step in determining $\mathcal{E}$ was to compute the fraction of these secondaries which gave counts in $N$ (shown as the shaded portion of the spectra in Fig. 13). This could be computed for each spectrum since the energy threshold (49 MeV) and the thickness (10.2 cm) of the NaI crystals were known. We now discuss this calculation for each secondary separately.

(1) *Gammas.* These high-energy gammas lose energy in the crystal by forming an electron shower. The cross section for pair production in the NaI could be calculated, and the amount of energy lost per unit length by an electron shower has been measured in this energy range.[44] For each energy interval in the spectrum, the minimum length, $x$, of the shower needed to leave $\geqslant 49$ MeV in the crystal was determined. The probability of forming a shower long enough in the crystal to be detected was then computed from $e^{-\mu(t-x)}$, where $t$ is the thickness of the crystal, and $\mu=\rho\sigma$, $\rho$ being the density of nuclei in NaI, and $\sigma$ being the pair production cross section (note in Fig. 13 that for gamma energies $<100$ MeV, we had $x>t$, and the showers could not leave enough energy in the crystal to be detected).

(2) *Negative pions.* All below 49 MeV stopped in the crystal and interacted. Those interactions yielding one or more charged particles would leave more than 49 MeV in the crystal and be detected. Those interactions yielding only neutrals were assumed not to register, since the probability for neutrals interacting in the crystal was small. The fraction of interactions yielding only neutrals was taken to be $(37\pm10)\%$, the same as the fraction of zero-pronged stars observed in pion interactions on heavy nuclei in emulsion.[45] For $\pi^-$ greater than 49 MeV, all were capable of being detected by ionization except for a small fraction interacting and yielding only neutrals.[46]

(3) *Positive pions.* All below 49 MeV stopped in the crystal and decayed. The coincidence resolving time was about 2 nsec, so the decay was not detected. All above 49 MeV were treated the same as $\pi^-$.

(4) *Protons.* All above 49 MeV registered by ionization energy loss.

(5) *Neutrons.* Those above 49 MeV which interacted in the crystal could register. The interaction cross section was taken to be geometric.

(6) *Multiple.* Since there was correlation between decay products of the same particle, and the total

[44] A. Kantz and R. Hofstadter, Phys. Rev. **89**, 607 (1953).
[45] G. Brown and I. S. Hughes, Phil. Mag. **2**, 777 (1957).
[46] The interaction cross section was taken from A. E. Ignatenko, A. I. Mukhin, E. B. Ozerov, and B. M. Pontecorvo, Zh. Eksperim. i Teor. Fiz. **31**, 546 (1956) [English transl.: Soviet Phys—JETP **4**, 351 (1957)]. The fraction yielding neutrals was taken to be the same as at rest. The magnitude of this correction was only 7.5%.

solid angle subtended by $N$ (4.8% of the sphere) was not small, events in which more than one secondary would intercept $N$ were tabulated separately in the Monte-Carlo calculation. The detection probability for these events was obtained from the appropriate combination of detection probabilities for the single events.

The final results for the calculation of $\mathcal{E}$ are given in Table V, where the contributions from each type of secondary are listed separately. The amount of uncertainty listed with each secondary includes the statistical uncertainty of the Monte-Carlo calculation, the effect of the uncertainty in the shape of the initial spectra used in the calculation, and an estimate of the systematic errors from the energy threshold determination and the calculated energy loss. In addition to these, two other effects are likely to have an important influence on the result: the effect of finite edges of the NaI crystals, and the scattering of particles from the walls of the lead shielding surrounding the crystals. The edge effect was estimated by comparing the solid angle subtended by the edges with that subtended by the entire crystal. This gave an estimated uncertainty of ±11%. An upper limit to the scattering from the walls of the lead shielding was estimated assuming isotropic scattering of all charged particles intercepting the walls. This gave a 4% increase to the total solid angle, so we have taken (2±2)% as an estimate of the increase in the efficiency from this effect. The fraction of gammas forming showers in the walls which give addisional counts in the crystals is expected to be negligible, tince the widths of the showers[44] are small.

TABLE V. A summary of the calculated efficiency for detecting stopping $K^-$ by counting secondaries with the NaI detectors. The estimated uncertainty in the total value includes the uncertainty listed for each secondary plus estimates of edge effects in the detectors and scattering from the surrounding shielding (see text). The uncertainties have been combined in quadrature.

| Type of secondary | Number detected per stopped $K^-$ |
|---|---|
| $\gamma$ | 0.0105±0.0005 |
| $\pi^-$(<49 MeV) | 0.0104±0.0016 |
| $\pi^-$(>49 MeV) | 0.0225±0.0016 |
| $\pi^+$ | 0.0047±0.0004 |
| $p$ | 0.0060±0.0003 |
| $n$ | 0.0012±0.0001 |
| multiple | 0.0077±0.0004 |
| Total | 0.0630±0.0076 |

PHYSICAL REVIEW VOLUME 158, NUMBER 5 25 JUNE 1967

# Two-Prong + $K_1^0$ Events in $K^-d$ Interactions at 2.24 BeV/$c$†

K. F. GALLOWAY, R. J. DEREMER,* E. D. ALYEA, JR., R. R. CRITTENDEN, H. J. MARTIN, JR., AND J. H. SCANDRETT‡
*Indiana University, Bloomington, Indiana*
(Received 13 January 1967)

A total of 702 events with two charged particles and a $K_1^0$ meson in the final state have been measured. Three hundred and eighty-five of these events represented the $K^-d \to \bar{K}^0\pi^- pn$ reaction and they have been divided, using the spectator model, into 247 $K^-p \to \bar{K}^0 p\pi^-$ events and 138 $K^-n \to \bar{K}^0\pi^- n$ events. Both reactions show resonance production. The $K^-p \to \bar{K}^0\pi^- p$ reaction has (56±5)% $K^{*-}p$ final state; the $K^-n \to \bar{K}^0\pi^- n$ reaction has equal $N^{*-}$ and $K^{*-}$ production, (26±8)% $K^{*-}n$ in the final state and (25±8)% $\bar{K}^0 N^{*-}$. Angular distributions and information on other final states are also given.

## INTRODUCTION

THE work presented in this paper is part of a bubble-chamber study of $K^-$ mesons interacting in deuterium at 2.24 BeV/$c$. The data include all events with two charged particles and a $K_1^0$ meson in the final state. This final state is dominated by the $K^-d \to \bar{K}^0\pi^- pn$ reaction and its experimental features are consistent with an impulse approximation model in which the incident beam interacts with only one of the nucleons in the deuteron. Results on the $K^-p \to \bar{K}^0\pi^- p$ and the $K^-n \to \bar{K}^0\pi^- n$ reactions have been extracted from the data and a comparison of these reactions is given.

Experimental studies of the $K^-p \to \bar{K}^0\pi^- p$ reaction at several beam energies show that the final state is dominated by the $K^*$(891 MeV) resonance and that the production and decay characteristics of this resonance are consistent with a production model involving one-meson exchange. Isospin considerations within the framework of this exchange model indicate that $K^{*-}$ production in the $K^-n$ and $K^-p$ reactions should be similar. There are, of course, differences between the two reactions and variations from the isospin predictions are expected. The results that will be presented here, although limited by statistics, indicate differences

† Supported in part by the National Science Foundation.
* Current address: Physics Department, San Bernadino State College, San Bernadino, California.
‡ Current address: Department of Physics, Washington University, St. Louis, Missouri.